

## Article

# Low-Cost Three-Quadrant Single Solar Cell *I-V* Tracer

José Ignacio Morales-Aragón<sup>1</sup> , Víctor Alonso Gómez<sup>1</sup> , Sara Gallardo-Saavedra<sup>2</sup> , Alberto Redondo-Plaza<sup>2</sup> ,  
Diego Fernández-Martínez<sup>2</sup> and Luis Hernández-Callejo<sup>3,\*</sup> 

<sup>1</sup> Departamento de Física, Universidad de Valladolid, 47002 Valladolid, Spain; zigurratt@coit.es (J.I.M.-A.); victor.alonso.gomez@uva.es (V.A.G.)

<sup>2</sup> Departamento Ingeniería Agrícola y Forestal, Universidad de Valladolid, 47002 Valladolid, Spain; s.gallardosaavedra@gmail.com (S.G.-S.); alberredon@gmail.com (A.R.-P.); diego-brivi@hotmail.com (D.F.-M.)

<sup>3</sup> ADIRE-ITAP, Departamento Ingeniería Agrícola y Forestal, Universidad de Valladolid, 47002 Valladolid, Spain

\* Correspondence: luis.hernandez.callejo@uva.es; Tel.: +34-975129418

**Abstract:** An *I-V* curve measurement technique is one of the most important techniques available for characterising photovoltaic cells. Measuring an accurate *I-V* curve at the single-cell level is a challenging task because of the low voltages and high currents implied, requiring the management of very low impedances. In this paper, the authors propose a low-cost device for *I-V* curve measurements of single (or small amounts) of cells in a series based on the charge transfer between two capacitors of equal capacitance. Our measurement strategy allows us to trace the usual first quadrant curve (the normal working region of solar cells) as well as the second and fourth quadrants of the *I-V* curve, which are quite important for research purposes. A prototype was built to demonstrate the feasibility and successful measurements of the three-quadrant *I-V* curve, obtained for more than 20 different cells. To use the device in a laboratory, without depending on the solar irradiation, a modular platform was 3D-printed, integrating a board with infrared LEDs as irradiating devices, and housing (to place the solar cell under test). The result is a useful low-cost setup for three-quadrant *I-V* curve tracing that works as expected.

**Keywords:** *I-V* curve; electroluminescence; photovoltaic; solar cell



**Citation:** Morales-Aragón, J.I.; Gómez, V.A.; Gallardo-Saavedra, S.; Redondo-Plaza, A.; Fernández-Martínez, D.; Hernández-Callejo, L. Low-Cost Three-Quadrant Single Solar Cell *I-V* Tracer. *Appl. Sci.* **2022**, *12*, 6623. <https://doi.org/10.3390/app12136623>

Academic Editors: Enrico Cagno, Mohsen Soltani, Edris Pouresmaeil and Pooya Davari

Received: 26 May 2022

Accepted: 28 June 2022

Published: 30 June 2022

**Publisher's Note:** MDPI stays neutral with regard to jurisdictional claims in published maps and institutional affiliations.



**Copyright:** © 2022 by the authors. Licensee MDPI, Basel, Switzerland. This article is an open access article distributed under the terms and conditions of the Creative Commons Attribution (CC BY) license (<https://creativecommons.org/licenses/by/4.0/>).

## 1. Introduction

There are many different techniques for characterising photovoltaic (PV) solar cells in various aspects. Some are focused on the microscopical compositions of the cells and the influences on their macroscopical behaviours; others are directly on these macroscopical aspects [1–5]. From a practical point of view, the cell is used to produce electricity; this may be the most important aspect. Of course, it is very important to know why cells do not perform as well as they should, what problems they currently experience, and how they may evolve. However, we first need to inspect them expeditiously and discover whether they are working as expected. For this purpose, there are techniques, such as electroluminescence (EL) imaging [6–8], thermal imaging [9,10], or the *I-V* curve. The latter is the only one that can directly show the output power of the PV cell with certainty because it measurements the variation of the current flowing through the cell when the voltages across the terminals are forced to change (that is, when the load resistance connected at the output changes). It is not possible to trace the *I-V* curve of a single cell in a commercial PV module (just the full module *I-V* curve). Nonetheless, it is possible in a laboratory to use single cells instead of complete modules. This information (at the cell level) is interesting for research purposes and can be used by manufacturers to detect bad cells and discard them before integration into a module, or classify them and put similar cells into a module to avoid mismatching [11].

Various topologies are used to measure the *I-V* curve, based on different ways of varying the loads seen by the PV cell or module [12]. Most commercial devices use variable

loads or capacitor charges to trace the  $I$ - $V$  curve. Regarding the systems that are based on various resistive loads, most are designed for standard modules (usually over 60 cells in series) or for an array of modules (usually about 30 modules), where the voltages are in the order of tens or hundreds of volts, and the load resistances are relatively easy to manage. The main difficulty in accurately measuring the  $I$ - $V$  curve of a single cell by varying the load is that the voltages implied are very low (less than 1 V) while the currents can be relatively high (in the order of 10 A). With these numbers, Ohm's law yields that we have to manage the load resistances in the order of  $0.1 \Omega$  or less. In these conditions, achieving the zero-voltage point could be a tough task since any parasitic resistances along the current path will prevent the cell from reaching this point.

For example, if we are measuring  $I$ - $V$  curve points at  $I = 10$  A and  $V = 0.1$  V, an equivalent resistance in the total circuit lower than  $10 \text{ m}\Omega$  is needed. Most contact resistances of usual probes, such as the ones in regular multimeters, cable connectors, etc., are higher than this value. Many strategies can be used to solve this: high section cables, soldered connections, wide copper tracks at printed circuit boards (PCBs), short electric paths, gold plated connectors, etc.

As will be shown in the following section, these problems are overcome by the special configuration of our circuit: they naturally force voltages across the solar cell from reverse to forward polarizations, inevitably crossing the zero voltage point regardless of the parasitic resistance of the current path, with the added benefits of being very cheap (compared to professional commercial devices) and the possibility of obtaining the complete  $I$ - $V$  curve (first, second, and fourth quadrants) of the PV cells measured. Moreover, the electronics can easily be adjusted to measure a small number of cells in a series association (small module) by modifying only the value of a pair of resistors on the PCB.

The article is organised as follows: Section 2 presents the method used as well as the available materials. Section 3 presents the results of the scientific work. Section 4 presents the discussion. Section 5 presents the conclusions drawn from the scientific work.

## 2. Methods and Materials

### 2.1. Solar Cell $I$ - $V$ Curve Characteristics

The general  $I$ - $V$  curve characteristics of a solar cell are well known and can be predicted from the simplest electrical model, namely the one-diode model (Figure 1).

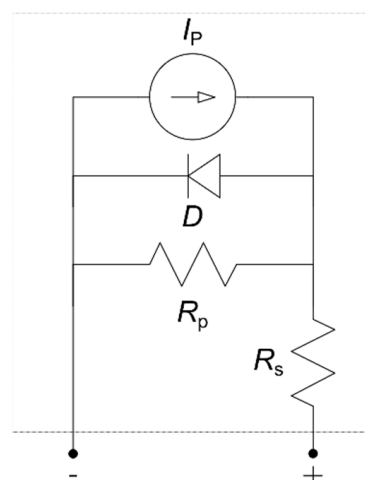


**Figure 1.** One-diode model for a photovoltaic cell.  $I_p$ : current source;  $D$ : diode;  $R_p$ : parallel resistor;  $R_s$ : series resistor.

Within this model, a current source ( $I_p$ ) is used to consider the photogenerated current of the solar cell and a diode ( $D$ ) to model the fact that a cell is, in essence, a P-N junction between two semiconductors. Finally, a parallel resistor ( $R_p$ ) and a series resistor ( $R_s$ ) model show that the diode and the source are not ideals (contact resistances, impurities,

annihilation between conduction electrons and holes, scattering, and collisions with the crystalline net, etc.).

Since the usual  $R_p$  has a very high value and the  $R_s$  has a low one, from this model it is easy to induce that, for moderate reverse voltages or forward ones under the conduction voltages of the diode, the external current is approximately equal to  $I_p$  (the forward current), since the diode is in an off-state and no (or very small) currents flow through it. This region corresponds to the flat sections within the first and second quadrants of the curve in Figure 2b, where the  $I_p$  is labelled as  $I_{SC}$  (solar cell short circuit current), as they are the same. However, if the reverse voltage is applied enough, the avalanche (Zener) voltage of the diode could be reached and the reverse avalanche current through the diode will be added to the forward external current, resulting in currents rapidly increasing over the  $I_p$  value (the left region of the curve (b) in Figure 2). On the forward voltage side, if the conduction voltage of the diode is reached, the forward current through the diode will be subtracted from  $I_p$ , and the output current will be reduced. From this point, if the forward voltage continues to rise, the output current will reach zero and will even be reversed, exponentially, to negative values, corresponding to the right region of the curve in Figure 2b, within the first and fourth quadrants.

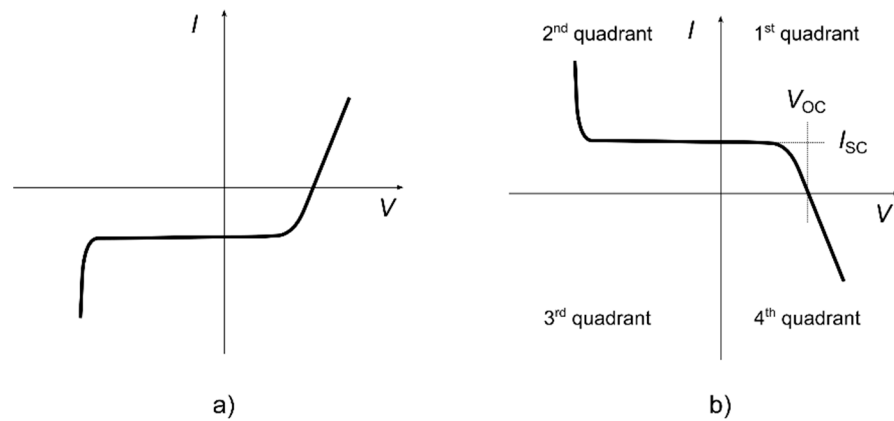


**Figure 2.** *I-V* curve of a photovoltaic cell. (a) Maintaining the current and voltage criteria from the diode. (b) Inverting the current criterion from the diode.  $V_{OC}$ : open circuit voltage;  $I_{SC}$ : short circuit current.

### 2.2. Principles of Operation

As shown in Figure 3, the proposed *I-V* tracer is just based on the current transfer between two capacitors of equal capacitances across a solar cell.

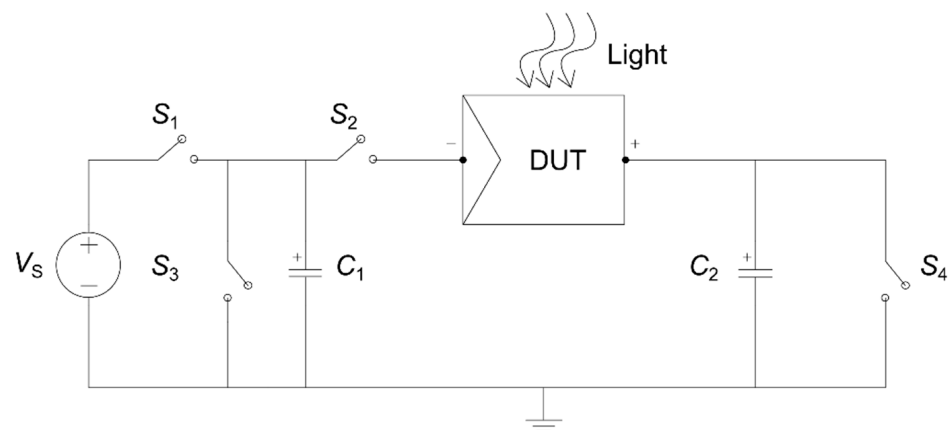


**Figure 3.** Schematic topology for the proposed *I-V* tracer. DUT: device under test.

Our design for the three-quadrant  $I$ - $V$  tracing takes advantage of the fact that most of the curve (from the second quadrant at the left to the zero current point in the first quadrant) corresponds to positive (forward) values of the current and, for a wide range of voltage values, is approximately constant in the current.

If we connect our solar cell under test to the positive plates of these capacitors, a forward current gives rise to a charge transfer from one capacitor to another and, consequently, the voltages change (one rises and the other diminishes). The changing rate of one capacitor voltage is expressed as shown (1):

$$\frac{dV}{dt} = \frac{I}{C} \quad (1)$$

So, as the capacitances of both capacitors are the same, their voltage changing rates are the same, with one rising and the other reducing, proportional to the current. Considering that the voltages across the solar cells are the differences of the voltages across each capacitor, these will vary at rates proportional to the currents. This means that, if we start from a difference between the capacitor voltages representing an initial reverse voltage for the cell, we will stand on the flat region of the curve; the solar cell voltage evolution will be (more or less) a linear sweep (as shown in Figure 23 below). As the cell voltage reaches values next to  $V_{OC}$ , the cell current diminishes, and the voltage sweep speed slows down (as shown in Figure 22 below). This way, a voltage sweep will be performed naturally, with the curve traveling from the beginning negative voltage in the second quadrant to near the zero current (positive voltage  $V_{OC}$ ) point, where the charge transfer will stop, and the voltage sweep finishes.

To trace the fourth quadrant section of the curve, another voltage sweep needs to be performed (in this case, starting from an initial cell voltage over  $V_{OC}$  and finishing again on  $V_{OC}$ ). After these two voltage sweeps, we will have traced a complete three-quadrant solar cell curve.

The measurement strategy could also be carried out on small associations of solar cells in series (small modules) and even regular photovoltaic modules (PV modules). For this reason, we designate it as the device under test (DUT).

#### Measurement process.

The process, controlled by opening or closing the needed switches at each step, is conducted as follows:

1. Firstly, both capacitors ( $C_1$  and  $C_2$ ) are discharged— $V(C_1) = V(C_2) = 0$ —and all switches ( $S_1$ ,  $S_2$ ,  $S_3$ , and  $S_4$ ) are opened.
2. Then, by closing  $S_1$ ,  $C_1$  is charged to the source voltage ( $V_S$ ). This voltage ( $V_S$ ), as will be explained later, will be the starting reverse voltage of the curve and could be conveniently adjusted.
3.  $S_1$  is then opened again. At this point,  $C_1$  stays charged at vs. and  $C_2$  is still discharged. So,  $V(C_1) = vs.$  and  $V(C_2) = 0$  V.
4.  $S_2$  is then closed; at this point, the voltage at the DUT terminal is the differential voltage between the positive plate of  $C_2$  and the positive plate of  $C_1$ —that is,  $V(\text{DUT}) = V(C_2) - V(C_1)$ —. That means a reverse polarisation of the solar cell, which, considering its expected behaviour (described in Section 2.1), will supply a current proportional to its irradiation flowing from  $C_1$  toward  $C_2$  and, consequently, increasing the  $C_2$  voltage and lowering the  $C_1$  voltage by means of the charge transfer. This current will only stop when the DUT reaches the open circuit forward polarisation voltage ( $V_{OC}$ ), so the first and second quadrant regions travel (including the zero-voltage point); at the end of this process, the first voltage sweep (as described before) will be over.
5. Now, to perform the second voltage sweep,  $S_2$  is opened, and immediately,  $S_3$  is closed. This discharges  $C_1$ , so  $V(C_1) = 0$  V. At this point,  $C_2$ , whose voltage increased by means of the charge transfer process, will remain charged.
6.  $S_2$  has closed again while  $S_3$  remains closed. Now, the negative side of the DUT will stand at ground level while its positive side will be at  $V(C_2)$ . In this case,  $V(\text{DUT})$

=  $V(C_2)-0$ , which, by design, is far higher than the  $V(DUT)_{OC}$ . The DUT is now forward-polarised beyond the open circuit point, and the current flows opposite to the previous cases, from  $C_2$  to the ground until  $V(DUT)_{OC}$  is reached (decreasing from higher voltages). Consequently, the DUT is forced to travel the fourth quadrant of its  $I-V$  curve at this step.

7. Once the process ends and the current stops flowing,  $S_4$  is closed to discharge  $C_2$  completely, leaving the apparatus ready to start a new measurement from step 1 ( $S_4$  has opened again after the discharge).

**Tracing the  $I-V$  curve of a photovoltaic cell.**

Step 4 of the described process is the beginning of the tracing. With the capacitor  $C_1$  charged to the source voltage ( $V_S$ ) and the capacitor  $C_2$  totally discharged, we apply a positive voltage at the negative terminal of the PV cell and zero to the positive terminal; that is, a negative voltage (see Figure 2b). The starting negative value of the voltage is equal to  $-V_S$ , so by adjusting this source voltage it is possible to start the tracing at any desired point—even capturing the avalanche zone in the right region of Figure 2b. In this case, the current will flow inside the cell mostly through the current source since the diode is reverse-biased and the parallel resistance should ideally be very high (see Figure 4a). If the avalanche zone of the diode is reached with  $-V_S$ , the reverse current in the diode will be added to the cell current. Consequently, the current value is determined by the PV cell’s short-circuit current ( $I_{SC}$ ) with the possible addition of an avalanche current at the beginning of the trace. The discharge of  $C_1$  (due to this current) will produce the charge of  $C_2$ , or, equivalently, move to the right, along the  $I-V$  curve (see Figure 4b). When the voltage of both capacitors is equalised, the difference across the terminals of the cell will be 0 V; so in the  $I-V$  curve, it will be at the crossing point with the current axis ( $I_{SC}$ ). The cell will continue along its normal  $I-V$  curve until it reaches  $V_{OC}$ , where it cannot push more electrons outside itself—so,  $V(C_2) - V(C_1) = V_{OC}$ —. These assumptions and graphs are also applicable to the PV module. Indeed, a PV module is just a series association of single cells (sometimes there are also parallel associations) and some bypass diodes, so the effect over the  $I-V$  curve is just to multiply the  $V_{OC}$  by the number of cells in the series and the  $I_{SC}$  by the parallel lines (in case a parallel association exists). Of course, these assumptions are only valid if all the cells are equal and are in a good state. If there are bad cells, many deformations over the  $I-V$  curve occur, but the study of these cases is beyond the scope of this paper.

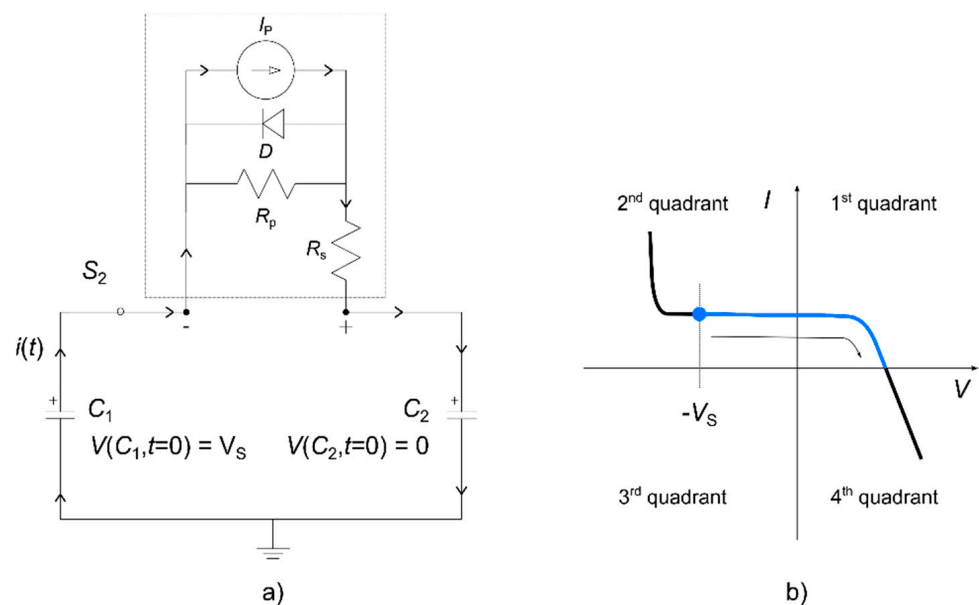


**Figure 4.** Step 4 of the process of measurements. (a) Equivalent circuit. (b) Path on the  $I-V$  curve.

After discharging the remaining charge in  $C_1$  at step 5, the capacitor  $C_2$  is positively charged—at about  $(V_S + V_{OC})/2$ , since the capacitances of  $C_1$  and  $C_2$  are equal, so when the switch  $S_2$  is closed at step 6, the PV cell is forced to jump to a state where a positive voltage is applied to its terminals (the fourth quadrant of its  $I$ - $V$  curve). If the starting voltage of the previous process ( $V_S$ ) is high enough, the remaining voltage in  $C_2$  will be higher than  $V_{OC}$ . Then, as can be seen in Figure 5a, the current will flow mostly across the diode (now polarised in the forward bias), because the photogenerated current goes in the opposite direction and the parallel resistance should be ideally very high. The current will flow until the potential difference at the ends of the diode reaches its forward conduction voltage. The  $V_{OC}$  of the PV cell now has a clear meaning—the voltage needs to put its own diode in conduction when the generated photo-charges flow across the P-N junction and annihilate. For this reason, it is impossible to overpass this point just by illuminating the cell; it must be forced with an external source. On the  $I$ - $V$  curve, the path followed will be to the left, until  $V_{OC}$  (see Figure 5b). Regarding the measurements of a PV module or serial associations of cells, the same reasons exposed before can be applied here; the process will be similar but with the voltages and/or currents raised.

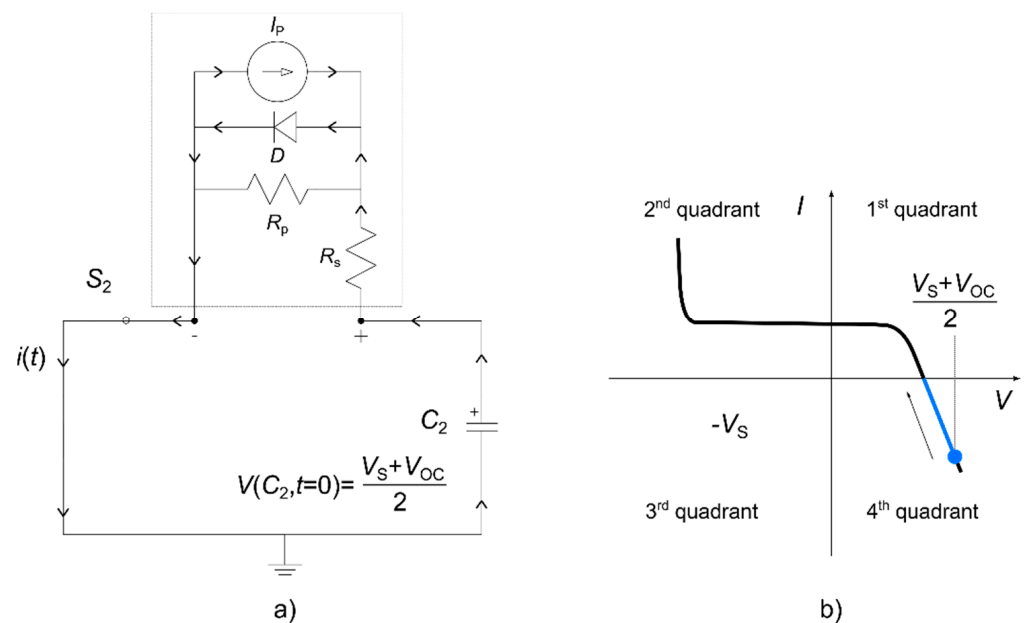


Figure 5. Step 6 of the process of the measurements. (a) Equivalent circuit. (b) Path on the  $I$ - $V$  curve.

### 2.3. Device Implementation

#### Time of the process and capacitance calculation.

The time spent in the charge transfer between  $C_1$  and  $C_2$  depends on the current flowing from the first to the second, as well as their capacitances. Of course, the higher the capacitances of both capacitors, the higher the time. The current depends on the technology fabrication of the PV cell and its efficiency, especially, on its surface area. For silicon technology (mono or polycrystalline) cells of common sizes today (around 160 by 160 mm),  $I_{SC}$  goes from 7 to 12 A, more or less (however, larger sizes are coming in future years). Current ( $I$ ) is related to charge ( $Q$ ) and time ( $t$ ) by its definition, and the voltage across the capacitors ( $V$ ) is obtained by dividing the charge stored ( $Q$ ) over the capacitance ( $C$ ), assuming a constant current process, as shown (2):

$$I = \frac{Q}{t}, V = \frac{Q}{C}, t = \frac{C \cdot V}{I} \tag{2}$$

In fact, the current in a general case is not strictly constant, especially if the avalanche zone is also traced, but this calculation can provide us with the order of magnitude of the

processing time for some chosen capacitances and voltages at the source. For a more precise estimation of the real-time, we simulate the circuit in LTSpice with the one-diode model for the DUT (see Figure 6), for the first voltage sweep.

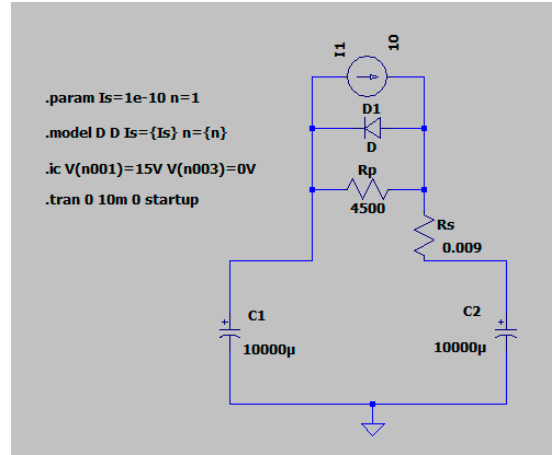


Figure 6. Circuit simulated in LTSpice for estimating the necessary capacitance for  $C_1$  and  $C_2$ .

As an example, for the circuit simulated in Figure 6, with an initial  $V(C_1) = 15\text{ V}$ ,  $V(C_2) = 0\text{ V}$ ,  $I(\text{DUT})_{SC} = 10\text{ A}$  and  $C_1 = C_2 = 10,000\ \mu\text{F}$  (with reasonable values for the diode characteristics, the parallel resistance, and the series resistance), the current flow and voltages at capacitors are shown in Figure 7. This simulation corresponds to the first voltage sweep described in Section 2.2. The second quadrant curve is traced from the starting point to the time where  $C_1$  and  $C_2$  voltage traces overlaps; that is,  $V(\text{DUT}) = 0\text{ V}$ , and then the usual  $I$ - $V$  curve of the PV device (first quadrant) is traced until the end of the sweep. We can appreciate better in Figure 8 how effectively the final voltages of both capacitors are not equal, but the difference is the  $V_{OC}$  of the measured cell. The total sweep time in this example is around 9.4 ms, and the capacitor voltage trace overlap occurs at 7.4 ms, so the usual  $I$ - $V$  curve in the first quadrant is travelled in about 2 ms.

For our prototype, we chose capacitors with capacitances of 22,000  $\mu\text{F}$  rated up to 40 V. This added to the use of PV cells with  $I_{SC} = 7.5\text{ A}$  and gave us more than double the amount of time to perform the measurements.

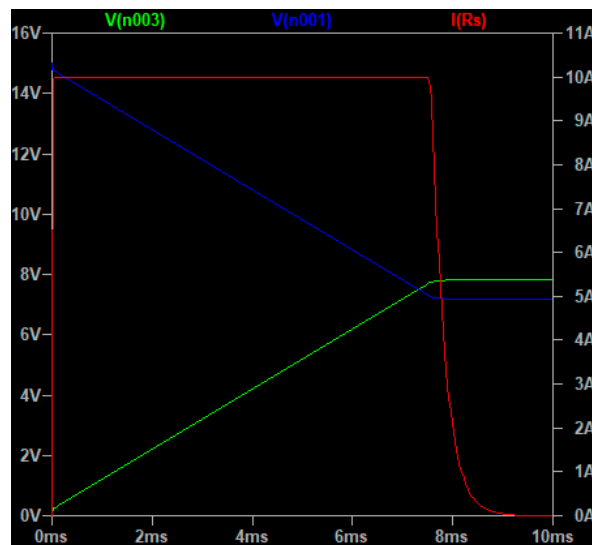
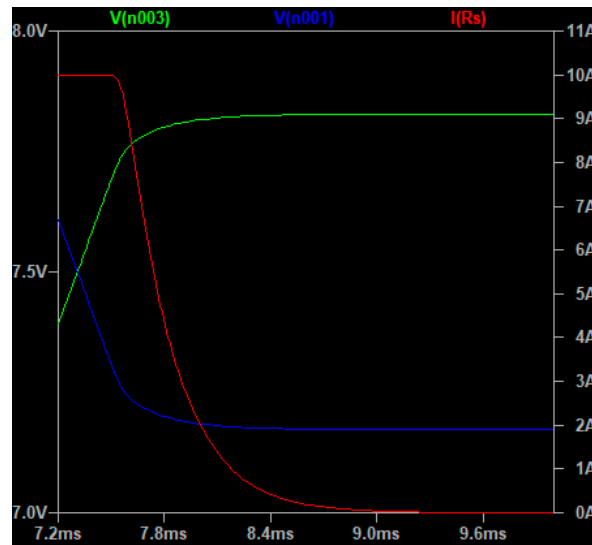
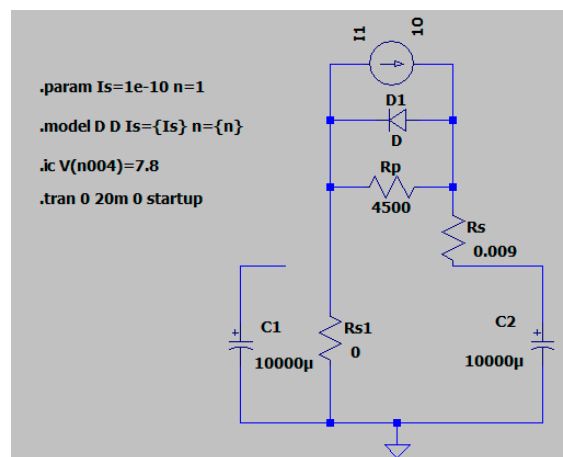


Figure 7. Time simulation for the discharge of  $C_1$  and the charge of  $C_2$  across the DUT. Current flow (red line), voltage of  $C_1$  (blue line), and voltage of  $C_2$  (green line) over time.



**Figure 8.** Zoomed graph of the most interesting zone of the discharge of  $C_1$  and the charge of  $C_2$  across the DUT. Current flow (red line), voltage of  $C_1$  (blue line), and voltage of  $C_2$  (green line) over time.

If we simulate in LTSpice the second voltage sweep (step 6 of the process, see Figure 9), we also obtain a time of around 2 ms (see Figure 10), but as shown in the figure, this implies currents of hundreds of amperes that will destroy the current sensor, so, to limit the reverse current for this measurement, an external resistor must be placed in series with the circuit. A shunt diode conducted in the forward current direction of the current avoids this series resistance for first sweep measurements. The effect of adding a resistor of  $0.3 \Omega$  is shown in Figure 11, where more moderate currents occur and the time spans 20 ms.



**Figure 9.** Circuit simulated in LTSpice for estimating the duration of step 6 of the process with the chosen capacitors and voltages.

### Prototype design.

For switch implementations, we selected metal oxide semiconductor field-effect transistor (MOSFET) devices controlled by a microcontroller (MCU) programmed adequately. The same integrated circuit (IC), a PIC16F1615, is capable of measuring voltages using a 10-bit analog-to-digital-converter (ADC) with eight multiplexed input channels. For the current measurements, a Hall-effect sensor IC (TMCS1100) in series with the current path was installed.

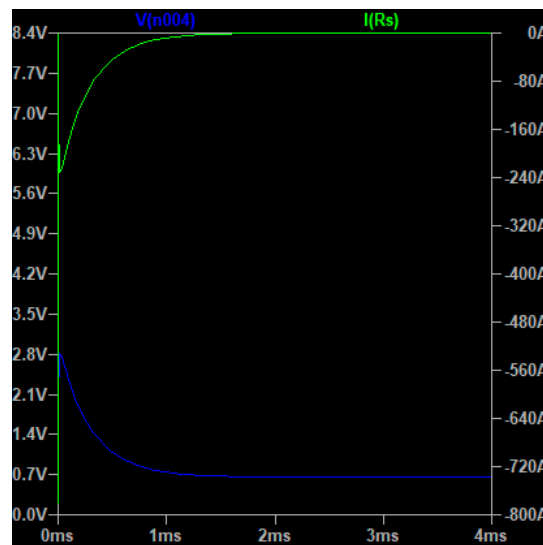


**Figure 10.** Time simulation for the discharge of  $C_2$  across the DUT without additional resistance. Current flow (green line), voltage of  $C_2$  (blue line) over time.

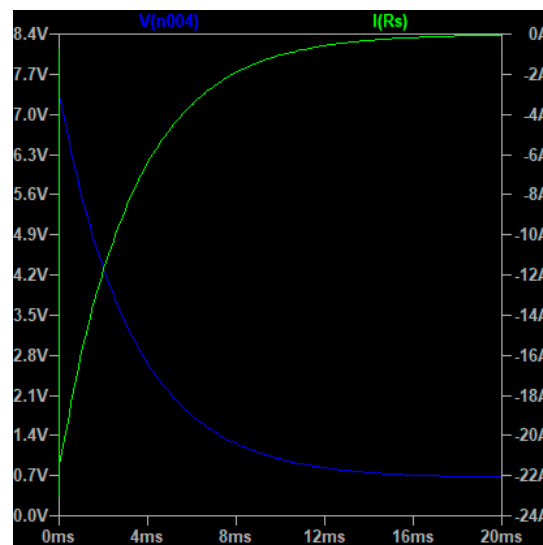


**Figure 11.** Time simulation for the discharge of  $C_2$  across the DUT with additional resistance of  $0.3 \Omega$ . Current flow (green line), voltage of  $C_2$  (blue line) over time.

This IC delivers an output voltage proportional to the current measured, in the range  $[0, 2.5)$  V for negative values of the current and in the range  $[2.5, 5]$  V for positive currents (including 0 A), and is rated to a maximum current of  $\pm 10$  A, delivering a voltage of 5 V in the case of +10 A and 0 V in the case of  $-10$  A. The voltage swing entering the ACD input must be 0 V to 5 V, so the current measurement IC can be directly connected to the analog input of the MCU, but for the voltage measurements, a voltage level adaptor circuit must be inserted. Voltages across the two capacitors ( $C_1$  and  $C_2$ ) determine the DUT voltage that we want to finally measure, so an operational amplifier (OA) fed with the two capacitor voltages at its inverting and non-inverting inputs will output the difference between them, adding gain or attenuation if desired, depending on the external resistors. For the full  $I$ - $V$  curve tracing, we must measure differential voltages, positive (on the first and fourth quadrants) and negative (on the second quadrant); the voltage swing in the first case—from 0 V to around (0.6–0.8) V—is much smaller than in the second one—from 0 V to vs. around (10–15) V. In addition, a good resolution is desirable in the usual first quadrant section of the curve, just where the voltage swing is smaller. For this reason, two different level adaptors

have been designed for each section, both with output voltage swings from 0 to 5 V: the first amplifying OA without inversion, with an input active differential voltage from 0 to 0.8 V for the positive adaptive voltages, and the second attenuating OA with inversion, with an input active differential voltage from  $-15$  to 0 V for the negative adaptive voltages. Two of the ADC multiplexer inputs are connected to the outputs of the OA level adaptors described and the firmware within the MCU will select the proper input depending on the section of the curve being measured. The detection of the zero-voltage point crossing will be the decision point for the MCU (for switching one channel to another). Figure 12 shows the connections of the OA level adaptors (without external resistors for simplicity) and the current sensor IC.

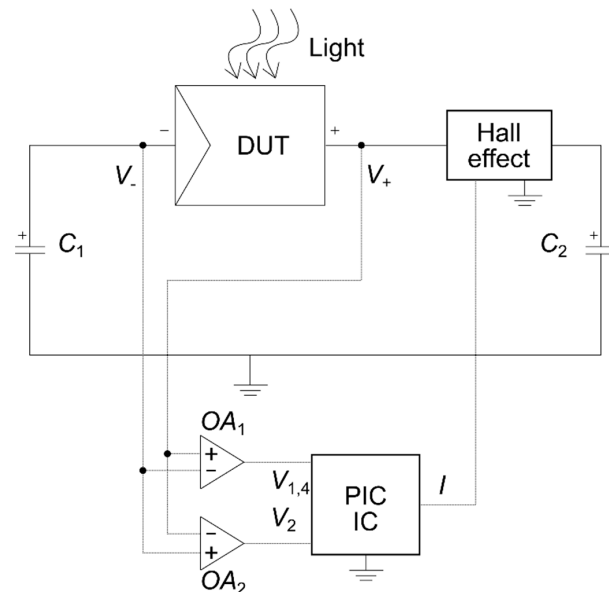


**Figure 12.** Voltage and current measure schematic for the  $I$ - $V$  tracer.

The scheme used to measure the voltage and current is shown in Figure 12. For the voltage across the solar cell, four-terminal sensing is used to determine it with enough precision. This concept must be transferred to the PCB design and the cables soldered to the DUT (using independent wires for the current and for the voltage to ensure a correct Kelvin sensing).

As soon as the MCU finishes the MOSFET (switches) sequence described in Section 2.2 (to start the first voltage sweep), it selects the proper ADC channel (the negative voltages level adaptor) and starts sampling voltage/current points. For the sake of a proper sampling speed, these pairs of current/voltage samples (10 bits of resolution each) are stored within the internal EEPROM memory of the MCU. When the MCU detects the zero-voltage point, it switches to the positive voltage ADC channel and continues sampling. Finally, the detection of the current samples close enough to zero indicates the first sweep end, and then the MCU performs the MOSFET switches sequence to start the second voltage sweep corresponding to negative values of the current. The sampling continues until the zero current point is detected again (the fourth quadrant section of the curve is traced with decreasing values of the voltage), and the full  $I$ - $V$  tracing is over. At this moment, all the samples stored in the internal MCU memory are dumped to an external host via the RS232 serial port integrated within the MCU, where they will be properly scaled and plotted, and the device will be ready for another tracing.

For all these tasks, we used a cheap 8-bit MCU that had an internal clock of 32 MHz, a maximum sampling rate of 100,000 samples/s, and an internal EEPROM memory capable of 500 samples (10 bits of resolution each). As we mentioned before, it is desirable to achieve a better resolution in the first quadrant section of the curve, since it is the natural working area of the cell, so an adaptive resolution was programmed in the MCU firmware

in such a way that the speed of sampling is higher in this section than in the others. This adaptive sampling could also be capable of taking curve points evenly distributed along the curve, even when the variations in the current in some sections during the sweeps lead to different sweeping speeds. Of course, the behaviour of the sampling could be adjusted as needed, or even modified from the host via RS232 commands. The most critical section for the sampling speed is the positive voltage one, where the current is close to  $I_{SC}$  and a large resolution is required. We mentioned before that for our prototype the sweep time for this region of the curve was in the order of 1 to 2 ms, with a maximum sampling speed of the MCU (100,000 samples/s), so we could take between 100 and 200 samples for this small (but interesting) region of the curve, which was between a quarter and a half of the internal memory capacity; this setup allowed us to have a reasonable sample distribution along the curve.

#### 2.4. Modular Platform Used

A modular platform was designed and used to help place the cell and the illumination LED board. The design was made using Autodesk Fusion 360 and then 3D-printed using fused filament fabrication (FFF) technology. In Figure 13, two configurations of the platform can be seen—the base with the adapters for the (156 × 156) mm cells and the supporting rods in (a); and with the adapter for the LED illumination board used in (b). Bigger cells, up to M6—(166 × 166) mm—are possible with this design. For future trend sizes, such as M8—(182 × 182) mm—or M10—(210 × 210) mm—a redesign of the platform will be needed. A picture of the prototype can be seen in Figure 14 along with the *I-V* tracer device.

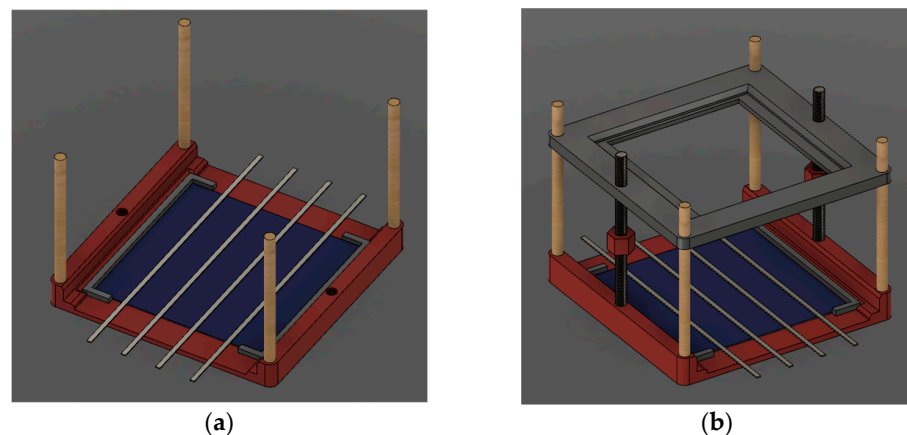


**Figure 13.** Modular platform designed for the measurement of *I-V* curves, electroluminescence, thermography, and other techniques. (a) Base with the cell and adapters. (b) With the addon for supporting the LED illumination board.

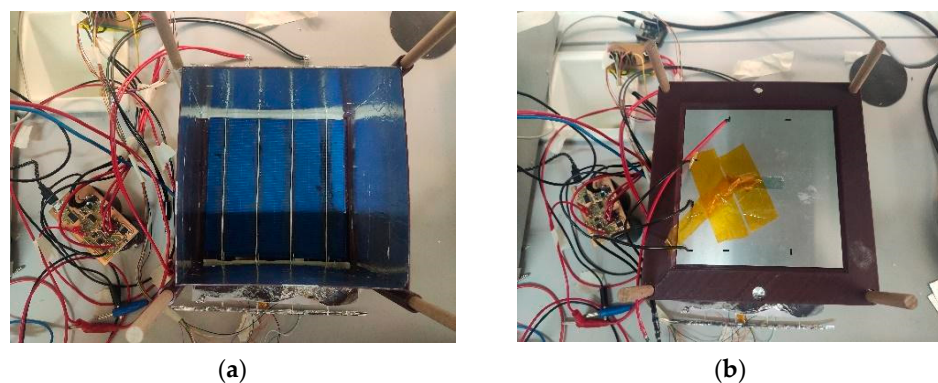


**Figure 14.** Modular platform mounted in the *I-V* tracer mode. (a) Assembled except for the LED board. (b) Fully assembled with the LED board in place.

### PV cells and LED illumination.

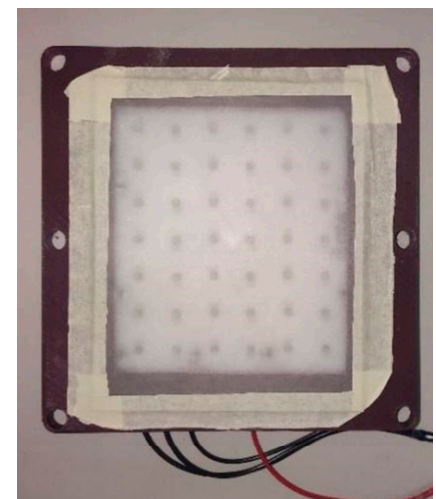
The characteristics of the PV cells used for testing are in Table 1. Busbars were hand-soldered to the cells using a soldering iron with the help of flux and hot air at 150 °C (see Figure 15a). The four busbars were then connected using a wider bar, which offered a low resistance path for the current and an easy zone to solder the voltage and current cables. Three cables were soldered at different points of each side (positive and negative) from the cell to the device to ensure the current flow with the lowest resistance possible. Another cable was soldered on each side for the voltage measurement.

**Table 1.** Technical characteristics of the PV cells used at nominal conditions (1000 W/m<sup>2</sup> of solar spectrum and 25 °C).

Characteristic	Value
Max power (MPP)	4.67 W
$V_{OC}$	0.645 V
$I_{SC}$	8.99 A
$FF$	0.81
Efficiency	19%
Number of busbars	4
Size	(156 × 156) mm
Thickness	200 µm
Technology	Polycrystalline



(a)



(b)

**Figure 15.** (a) Photovoltaic cell used. (b) LED illumination system used.

The illumination system was composed of an aluminium PCB with 42 infrared (IR, 850 nm) LEDs—see Figure 15b. This wavelength was chosen because the photon absorption curve for a silicon PV cell had its maximum efficiency in the near-infrared (NIR) zone, as shown in Figure 16. When these photons illuminating the cell are at their peak wavelengths, they could absorb better, so less energy is needed to obtain a state at the cell similar to the nominal conditions (1000 W/m<sup>2</sup> with the spectral composition of the Sun's irradiance at Earth's surface). Under these irradiation conditions, the PV cell can generate the free charges needed to reach its saturation current and, consequently, walk around its own *I-V* curve. The calibration of the current needed on the LEDs for obtaining the right density of photons was conducted with a calibrated irradiation cell to obtain the same signal exposed to the Sun at nominal conditions.

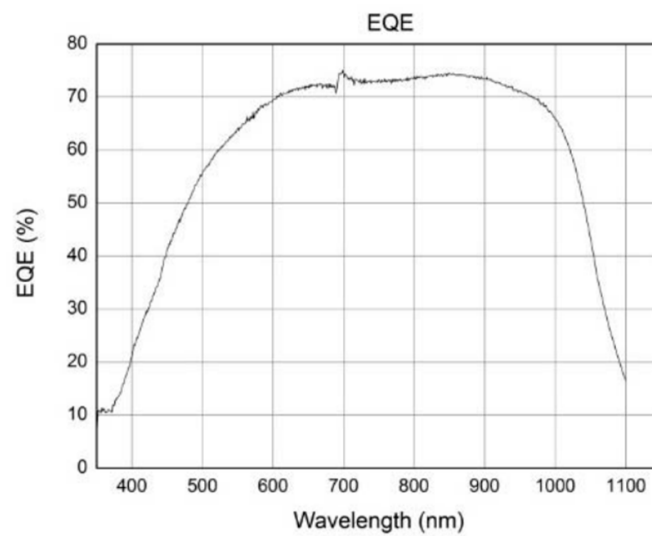


**Figure 16.** External quantum efficiency (EQE) of a silicon photovoltaic cell. Extracted from [13], our own elaboration.

### 3. Results

#### 3.1. Prototype Made

The actual implementation of the proposed  $I$ - $V$  tracer is displayed in Figure 17. Capacitors are placed behind the PCB, while the rest of the components are placed in the top layer. Moreover, the RS232 communication cable, the wires used to power the device and charge the capacitor, and the wires used to measure (independently) the current and voltage are shown. The technical characteristics are shown in Table 2.

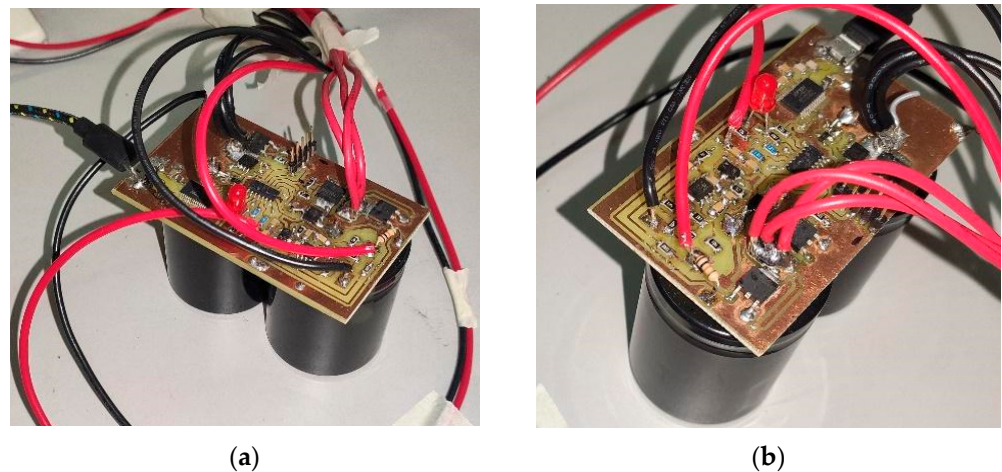


**Figure 17.** Prototype implementation of the proposed device.

**Table 2.** Technical characteristics of the device produced.

Characteristic	Value
Power voltage	15 V
Capacitance of $C_1$ and $C_2$	22,000 $\mu$ F
Current measure max ratings	$\pm 10$ A
Voltage measure max ratings	-15 V, +8.5 V
Number of points measured	248
Current resolution	25 mA
Voltage resolution	1 mV

### 3.2. *I-V* Curves Obtained

By means of the integrated serial RS232 port, the microcontroller can receive commands to configure the sampling range desired for the measurements. The first traces presented were configured to sample the first quadrant and a small section of the second one close to the zero-voltage point, obtaining the usual *I-V* curve in the generating region of the cell at a maximum resolution.

Figure 18 shows the graphical representation of the dataset acquired for a measure of a single PV cell, using our device for *I-V* tracing and the platform with the LED board for illuminating. The first quadrant (positive voltages) and some of the second quadrant (negative voltages) can be seen. The curve is the typical curve of a good cell, with the first zone at low voltages, almost horizontal; that is, without changes in the current (almost  $I_{SC}$ ) and then a “neck” zone ending in a straight zone up to the open circuit ( $V_{OC}$ ). From these values (at the beginning and the end), it could be possible to extract the values of  $R_p$  and  $R_s$ , respectively. The second quadrant of the curve is not traced because the firmware of the main IC is configured, in this case, to obtain the curve with the maximum number of points at the first quadrant zone.

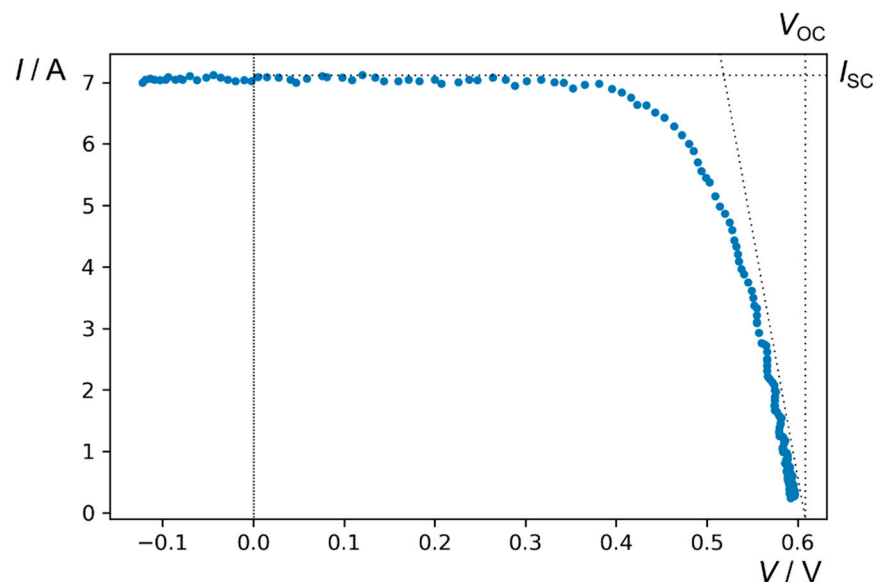


**Figure 18.** The *I-V* curve of a real cell with the device and the platform proposed for irradiance of  $750 \text{ W/m}^2$ .

As mentioned before, it is possible to also obtain an *I-V* curve with a small number of PV cells in series by simply changing the feedback loop of the voltage measure Op-amps. For this purpose, we fabricated a mini-PV module with six cells that were a sixth of a cell of the size used. Therefore, the mini-module could be mounted in a size just slightly larger than the single cell, so it fits in the modular platform and could also be illuminated with the same LED system. The corresponding *I-V* curve can be seen in Figure 19a. As expected, the noise in the current measure is more notorious in this case, because the values of the current are lower (the current depends mostly on the cell surface for the same cell technology). For this reason, a software Savitzky–Golay filter was used over the raw data. The filtered data are shown in Figure 19b.

For the full three quadrants, tracing the appropriate sampling range selection command was sent to the microcontroller. In this case, the two voltage sweeps described before were performed and the sampling covered the three-quadrant curve. Figure 20 shows the full *I-V* curve of the cell measured; we should note how the microcontroller had adjusted the sampling rate to perform a better resolution for the usually measured first quadrant, where more details were desired to extract the basic main parameters of the cell. More specifically, in the second quadrant and the first part of the first quadrant (from left to

right), the current was very high (so the variation in voltage was very fast) but the current variation was low (so the variation in the current was slow). Here, we could sample slower without loss of quality. After the change of the slope in the first quadrant, the situation was the contrary. The current was, at each step, lower, so the variation of the voltage was slower, but the variation in the current was faster, so we needed a faster sample rate. As explained in Figure 4, the curve was traversed naturally by the current flowing from one capacitor to the other, so the factor which determined the speed of the voltage variations in the capacitors was the current. Figure 21 shows a detail of this curve zoomed in to the first and fourth quadrants. In the figures, it can be appreciated that there is a *gap* between the positive and negative current sections. As mentioned before, it was impossible to reach the 0 V point (because the current tending to zero would result in time tending to infinite), but this was not a problem, because the *gap* data were easily interpolated from the tails of the two sections. This fact is shown in Figure 22, where the points of each curve from the first and fourth quadrants, which were close to the abscises axis (that is, close to  $V_{OC}$ ) were fitted to a second-degree polynomial. Consequently, one of the roots of this parabola was the interpolated value of  $V_{OC}$ . The coefficients of all those polynomials are not shown in this work because they were not useful for purposes other than the calculus of  $V_{OC}$ , but it is obvious from their representations in Figure 22 (dotted lines) that the experimental point in this zone has a parabolic form (which is also reflected in the regression coefficients  $r^2 > 0.99$  values obtained in the fit of each curve).

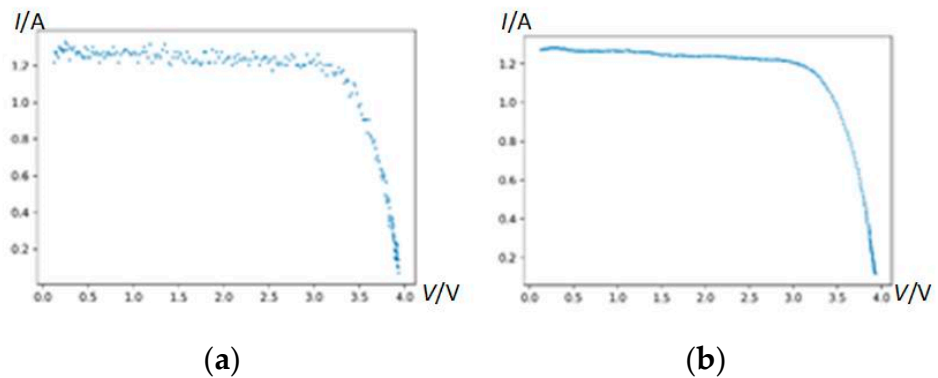


Figure 19. The  $I$ - $V$  curve of the mini-PV module of six single cells fabricated. (a) Raw data. (b) Filtered data.

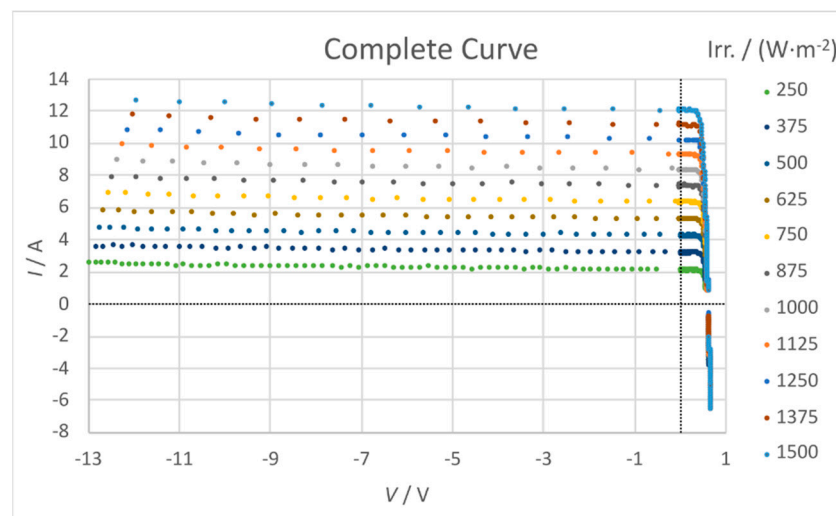


Figure 20. Three-quadrant  $I$ - $V$  curves measured with the prototypes at different irradiances from 250 to 1500  $W/m^2$ .

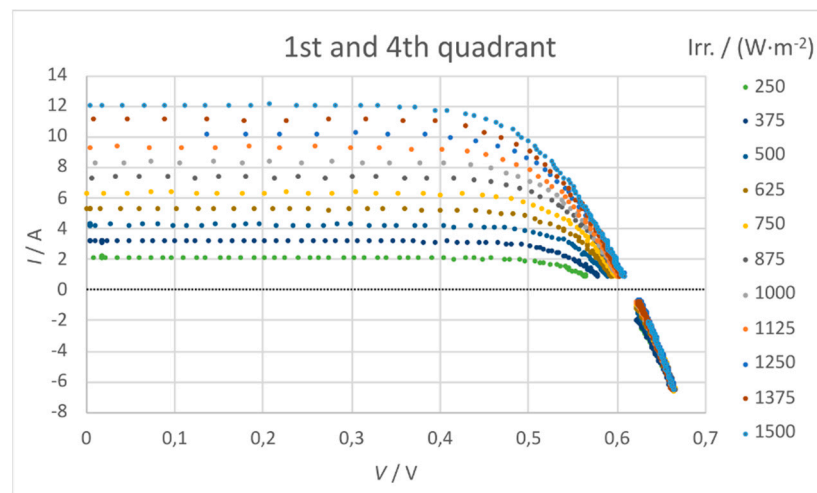


Figure 21. Details of the same  $I$ - $V$  curve (Figure 20) corresponding to the first and fourth quadrants.

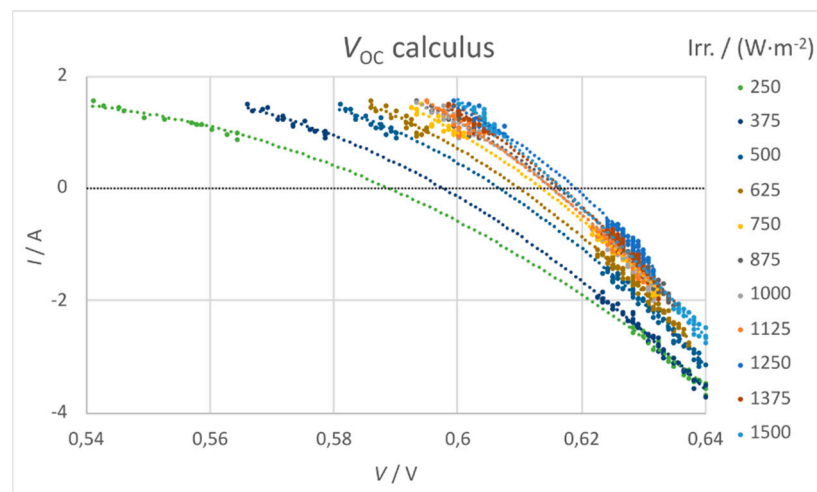


Figure 22. Details of the same  $I$ - $V$  curve (Figure 20) near the abscise axis intersection with the second-degree polynomial fit of the points of each curve for the calculus of  $V_{OC}$ .

All relevant parameters obtained from the experimental curves shown in Figures 20–22 are shown in Table 3.

Table 3. Technical characteristics of the PV cells used at nominal conditions (1000  $W/m^2$  of solar spectrum and 25 °C).

<i>Irradiance</i> / $W \cdot m^{-2}$	$V_{OC}/V$	$I_{SC}/A$	$P_{MPP}/W$	$FF/\%$
250	0.589	2.15	0.98	77.26
375	0.598	3.24	1.46	75.39
500	0.607	4.30	1.94	74.14
625	0.610	5.32	2.40	73.78
750	0.614	6.36	2.86	73.27
875	0.616	7.33	3.27	72.33
<b>1000</b>	<b>0.615</b>	<b>8.35</b>	<b>3.63</b>	<b>70.67</b>
1125	0.616	9.35	4.03	69.97
1250	0.619	10.21	4.41	69.79
1375	0.617	11.13	4.68	68.19
1500	0.617	12.09	5.06	67.84

Figure 23 shows the voltage sweep in the first quadrant (voltage vs. time); the sweep is maintained until the cell voltage reaches values next to  $V_{oc}$ , where the sweep speed slows

down due to the current falling. Figure 24 shows the voltage sweep in the second quadrant (voltage vs. time), the almost constant current in this section leads to a voltage sweep very close to linear.

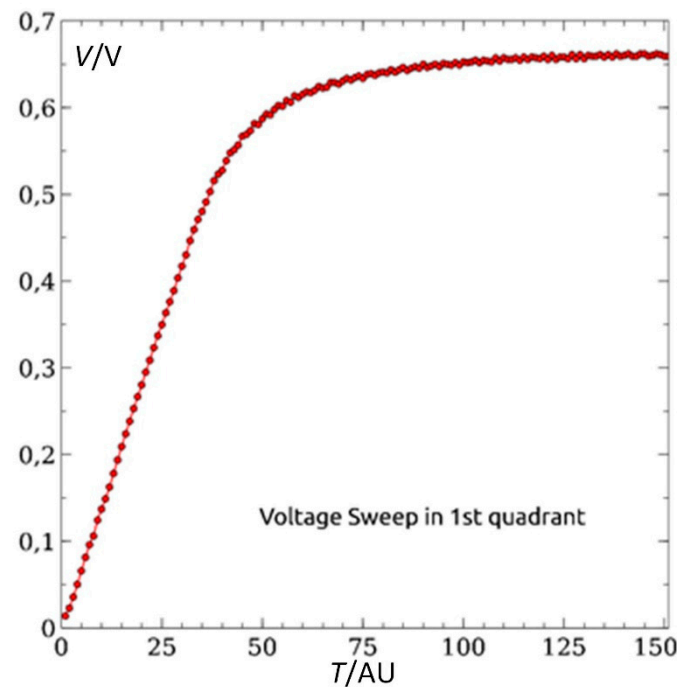


Figure 23. Voltage sweep in the first quadrant (voltage vs. time). AU: arbitrary units.

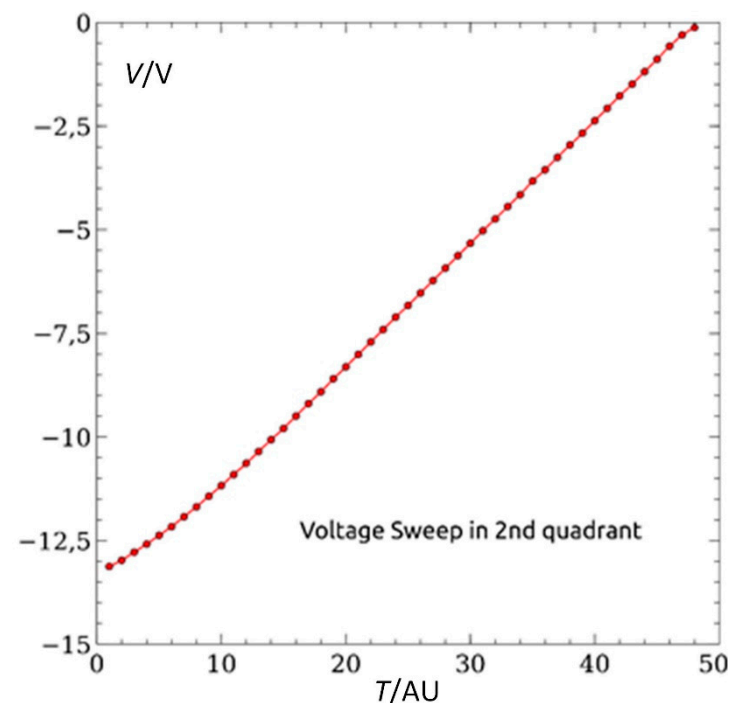


Figure 24. Voltage sweep in the second quadrant (voltage vs. time). AU: arbitrary units.

#### 4. Discussion

We demonstrated that the construction of a prototype based on our theoretical strategy is practically achievable and leads to a successful  $I$ - $V$  curve tracing of a single cell as well as a small number of cells. We solved the technical challenges encountered for the correct measurements of the voltage and current of the cell and designed all the electronics

needed to ensure it. The OA level adaptor ranges were adjusted and measured against an oscilloscope for a proper conversion from the ADC values to the actual voltage values. All the sign/scale conversions that were needed to correctly interpret the raw sampled data were conducted via software on a computer program. The data were downloaded from the device; the files were saved and plotted. We have not introduced this program, written by us in Python, because it could be conducted in many ways and is now very simple (without an interface, just in the command line mode).

The device was used to measure curves in more than 20 different single cells by the time (plus two mini-PV modules). These cells were of the same manufacturer and type as described in Table 1. The purpose of these measurements, in addition to demonstrating the validity of the apparatus, was to train an artificial intelligence (AI) algorithm along with its corresponding EL images, to classify cells into some groups according to their output power. These kinds of data are very difficult to obtain for the same cell, so a device such as this enables anyone to do it at a very low cost.

*I-V* tracers capable of taking good measurements at the cell level are in the price range of one thousand dollars (USD 1000) or higher. Some laboratories make them manually with two good multimeters and a programmable electronic load or via the one-capacitor charging method. One of these bank multimeters is in the range of one thousand dollars or higher, so the full equipment for an *I-V* curve could cost around USD 3000 or higher. The components used in our device cost around fifty dollars (USD 50). Obviously, we did not charge the costs for the design, make, mounting, programming, calibrating, testing, etc. The LED illumination board components cost less than one hundred dollars (USD 100) and the 3D-printed platform cost is derisory (USD 10 in filament or less, plus the electricity consumption).

The noise environment in our laboratory is quite severe, and it is expected to be more or less the same in the usual spaces where the device is intended to be used, so electromagnetic-superimposed noise was observed over the signal in the current measurements, but it did not seriously affect the shapes of the curves and could easily be eliminated by post-processing filtering.

We obtained a very promising result but, as in all processes (from theory to reality), some problems arose. The first was expected and related to the illumination. It is not exactly the same to illuminate a cell with the Sun spectrum as with a single wavelength. The biggest problem with the LED board is that we needed to place it relatively close to the cell (about 10 to 15 cm) to obtain an adequate signal. At this distance, it is difficult to obtain a homogeneous irradiance at the full cell area. Each LED is a big spot with a spatial irradiation cone. To minimise this problem, a diffuser was placed below the LEDs. Even so, as can be seen in Table 3, the  $I_{SC}$  obtained by us at a (supposed) irradiance of  $1000 \text{ W/m}^2$  was 8.35 A, while it should ideally be 8.99 A (from the manufacturer datasheet). This is just 7% less, but it evidences that the illumination in the cell plane is not homogeneous enough, which is also obvious from the maximum power point obtained, 3.63 W experimentally versus the theoretical 4.65 W (a 22% less). The most marked loss in power was due to the voltage and current drop compared to the theoretical at the maximum power point. Datasheet characteristics were obtained by the manufacturer in a flash test with homogeneous illumination, negligible warming, and very good contact probes that did not introduce the problems exposed here. Our thought was that the series and parallel resistance of the cell were raised after our manual soldering process of busbars, resulting in curves separated from the ideal. Busbar soldering is not easy. The very high thermal conductivity of the crystalline silicon and how easy it is to break the cell with any mechanical effort could result in bad soldering at some points, cold joints (with higher resistance), and small breaks. To minimizing that, hot air (for preheating) and flux were added, but it was very difficult to completely clean the residues after without the risk of breaking the cell. All those things, mixed with the influence of the not-so-homogeneous illumination, resulted in experimental measurements that were not as close to the datasheet as we would have liked. However, the problem does not lie with the *I-V* tracer we propose

but with the cell soldering and illumination system. We are attempting to improve these aspects for future works.

Another problem derived from the proximity of the LEDs was the heat generated by them. It is well known that the  $I$ - $V$  curve of a PV cell depends not only on the irradiance but also on the temperature. The cell raises its own temperature due to the absorption of the photons. Part (but not all) of the energy of these photons is evacuated from the cell due to the current output from the electrons. To this temperature increase, we had to add temperature increments due to the self-heating of the LED board, which heats the air gap trapped in the platform used. This is not a problem for the temperature stability across an individual  $I$ - $V$  curve, because, as has been said, it is a fast process. However, its influence could be considered between successive measurements, as can be seen in Figure 25. For this purpose, six very small temperature sensors based on thermistors were added to the platform, capable of delivering the information needed for the calculation of the average temperature or even its distribution. These sensors will allow for characterizing the dependence on the temperature of  $V_{OC}$ ,  $I_{SC}$ , and power output. The effect on the total power output of the mini-module is shown in Figure 26, which corresponds to the power calculated from the data shown in Figure 25.

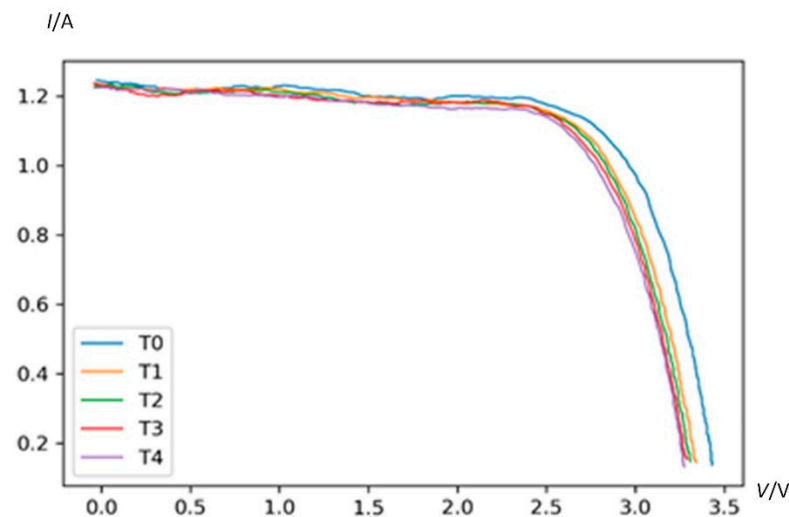


**Figure 25.**  $I$ - $V$  curves of a mini-PV module of six cells at different temperatures.  $T_0 < T_1 < T_2 < T_3 < T_4$ .

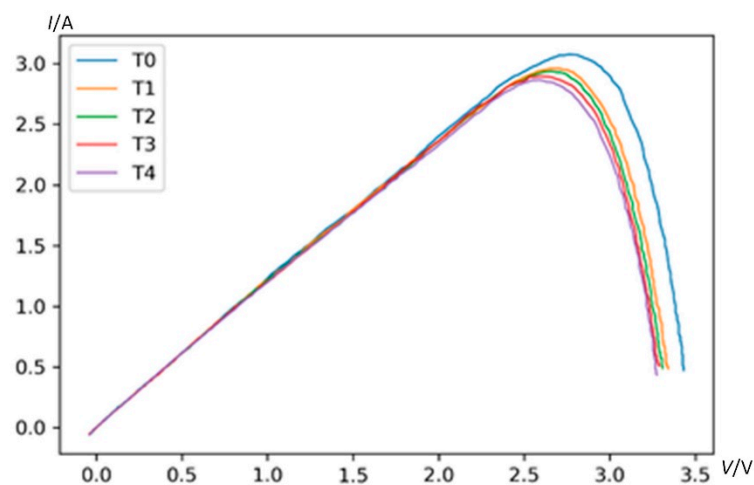


**Figure 26.**  $P$ - $V$  curves of a mini-PV module of six cells at different temperatures.  $T_0 < T_1 < T_2 < T_3 < T_4$ .

To incorporate all of these improvements, a new device is being designed using the most powerful MCU, with a faster clock, a 12-bit ADC, and much more internal memory

and processing power, which should be able to obtain more precise measurements and up to 5000 points at once, while also incorporating the temperature measurements. In addition, this new MCU will perform the communication with the computer over USB.

## 5. Conclusions

A new measurement strategy for an  $I$ - $V$  curve tracer at a single PV cell level, based on the charge exchange between two capacitors, was exposed. This strategy was successfully implemented in a low-cost device capable of doing these difficult measurements correctly. An illumination module based on NIR LEDs was also designed and built, demonstrating that this setup can be a good replacement for more complex and expensive systems.

All this equipment was integrated into a modular platform (designed and 3D-printed). This makes it possible to easily and quickly obtain a lot of  $I$ - $V$  curves for different conditions of illumination and/or shading. Data of this kind can be very helpful for training AI algorithms but are very difficult to obtain at the cell level. With this device and modular platform, we solved that problem in an easy and cheap way.

Future works will include a revised device, improving the quality of the measurement, reducing noise in the  $I$ - $V$  trace, and some new planned functionalities, such as scale changing without soldering, or simultaneous measurements of the temperatures of cells.

**Author Contributions:** Conceptualization, L.H.-C., J.I.M.-A. and V.A.G.; methodology, L.H.-C., J.I.M.-A. and V.A.G.; software, S.G.-S., A.R.-P., D.F.-M., J.I.M.-A. and V.A.G.; validation, J.I.M.-A. and V.A.G.; formal analysis, J.I.M.-A. and V.A.G.; investigation, L.H.-C., J.I.M.-A. and V.A.G.; resources, S.G.-S., A.R.-P., D.F.-M., J.I.M.-A. and V.A.G.; data curation, J.I.M.-A. and V.A.G.; writing—original draft preparation, L.H.-C., J.I.M.-A. and V.A.G.; writing—review and editing, L.H.-C., J.I.M.-A. and V.A.G.; visualization, S.G.-S., A.R.-P. and D.F.-M.; supervision, L.H.-C.; project administration, L.H.-C.; funding acquisition, L.H.-C. All authors have read and agreed to the published version of the manuscript.

**Funding:** CARACTERIZACIÓN AVANZADA DE CÉLULAS SOLARES Y MÓDULOS DE ALTA PRODUCTIVIDAD Y BAJO IMPACTO AMBIENTAL HACIA UNA ENERGÍA FOTOVOLTAICA VERDE, CIRCULAR Y SOSTENIBLE—GREASE”, Ref.: PID2020-113533RB-C33. Ministerio de Ciencia e Innovación (MCIN).

**Institutional Review Board Statement:** Not applicable.

**Informed Consent Statement:** Informed consent was obtained from all subjects involved in the study.

**Data Availability Statement:** Not applicable.

**Acknowledgments:** We would like to thank CEDER for providing information for the development of this work. The authors thank the CYTED Thematic Network “CIUDADES INTELIGENTES TOTALMENTE INTEGRALES, EFICIENTES Y SOSTENIBLES (CITIES)”, no. 518RT0558.

**Conflicts of Interest:** The authors declare no conflict of interest.

## References

1. Kwarikunda, N.; Van Dyk, E.E.; Vorster, F.J.; Okullo, W.; Munji, M.K. Application of LBIC Measurements for Characterisation of Triple Junction Solar Cells. *Phys. B Condens. Matter* **2014**, *439*, 122–125. [[CrossRef](#)]
2. Walter, J.; Eberlein, D.; Haunschild, J.; Tränitz, M.; Eitner, U. A Method to Detect Defective Solder Joints by RS-Electroluminescence Imaging. *Energy Procedia* **2012**, *27*, 652–657. [[CrossRef](#)]
3. Sinton, R.A.; Cuevas, A.; Stuckings, M. Quasi-Steady-State Photoconductance, a New Method for Solar Cell Material and Device Characterization. In Proceedings of the Twenty Fifth IEEE Photovoltaic Specialists Conference—1996, Washington, DC, USA, 13–17 May 1996; pp. 457–460. [[CrossRef](#)]
4. Breitenstein, O.; Frühauf, F.; Bauer, J. Advanced Local Characterization of Silicon Solar Cells. *Phys. Status Solidi* **2017**, *214*, 1700611. [[CrossRef](#)]
5. Fischer, S.; Goldschmidt, J.C.; Löper, P.; Bauer, G.H.; Brüggemann, R.; Krämer, K.; Biner, D.; Hermle, M.; Glunz, S.W. Enhancement of Silicon Solar Cell Efficiency by Upconversion: Optical and Electrical Characterization. *J. Appl. Phys.* **2010**, *108*, 044912. [[CrossRef](#)]

6. Bothe, K.; Pohl, P.; Schmidt, J.; Weber, T.; Altermatt, P.; Fischer, B.; Brendel, R. Electroluminescence Imaging as an In-Line Characterisation Tool for Solar Cell Production. In Proceedings of the 21st European Photovoltaic Solar Energy Conference, Dresden, Germany, 4–8 September 2006; WIP-Renewable Energies: München, Germany, 2006; pp. 597–600.
7. Fuyuki, T.; Kitiyanan, A. Photographic Diagnosis of Crystalline Silicon Solar Cells Utilizing Electroluminescence. *Appl. Phys. A* **2008**, *96*, 189–196. [[CrossRef](#)]
8. Gallardo-Saavedra, S.; Hernández-Callejo, L.; del Alonso-García, M.C.; Santos, J.D.; Morales-Aragonés, J.I.; Alonso-Gómez, V.; Moretón-Fernández, Á.; González-Rebollo, M.Á.; Martínez-Sacristán, O. Nondestructive Characterization of Solar PV Cells Defects by Means of Electroluminescence, Infrared Thermography, I–V Curves and Visual Tests: Experimental Study and Comparison. *Energy* **2020**, *205*, 117930. [[CrossRef](#)]
9. Dunlop, E.D.; Halton, D. Radiometric Pulse and Thermal Imaging Methods for the Detection of Physical Defects in Solar Cells and Si Wafers in a Production Environment. *Sol. Energy Mater. Sol. Cells* **2004**, *82*, 467–480. [[CrossRef](#)]
10. Johnston, S.W.; Call, N.J.; Phan, B.; Ahrenkiel, R.K. Applications of Imaging Techniques for Solar Cell Characterization. In Proceedings of the 2009 34th IEEE Photovoltaic Specialists Conference (PVSC), Philadelphia, PA, USA, 7–12 June 2009; pp. 276–281. [[CrossRef](#)]
11. Abete, A.; Barbisio, E.; Cane, F.; Demartini, P. Analysis of Photovoltaic Modules with Protection Diodes in Presence of Mismatching. In Proceedings of the IEEE Conference on Photovoltaic Specialists, Kissimmee, FL, USA, 21–25 May 1990; Volume 2, pp. 1005–1010. [[CrossRef](#)]
12. Zhu, Y.; Xiao, W. A Comprehensive Review of Topologies for Photovoltaic I–V Curve Tracer. *Sol. Energy* **2020**, *196*, 346–357. [[CrossRef](#)]
13. Ananda, W. External Quantum Efficiency Measurement of Solar Cell. In Proceedings of the 2017 15th International Conference on Quality in Research (QiR): International Symposium on Electrical and Computer Engineering, Nusa Dua, Indonesia, 24–27 July 2017; pp. 450–456. [[CrossRef](#)]